

Influence of Dynamic Processes upon Complete Fusion of Heavy Nuclei at Subbarrier Energies

M. Beckerman, M. K. Salomaa, J. Wiggins, and R. Rohe

Laboratory for Nuclear Science, Massachusetts Institute of Technology, Cambridge, Massachusetts 02139

(Received 29 November 1982)

Excitation functions for complete fusion of $^{90}\text{Zr} + ^{90}\text{Zr}$ and $^{90}\text{Zr} + ^{94}\text{Zr}$ have been found to decrease gradually over a broad energy range below the nominal barrier. The effective barrier for $^{90}\text{Zr} + ^{94}\text{Zr}$ was 10.5 ± 3.0 MeV higher than the nominal barrier implying a critical effective fissility of 31.5 ± 0.5 . Although deep-interpenetration processes appear to limit fusion at near-barrier energies, weak-contact dynamics enable these cold, heavy nuclei to fuse with comparative ease at lower energies.

PACS numbers: 25.70.Jj, 25.70.Gh

At energies not too far above the barrier, the fusion of two nuclei is presumed to be governed by the presence or absence of a pocket in the interaction potential, $V_i(r)$. When the pocket is present, and there is sufficient energy, $E_{c.m.}$, to overcome the outer maximum in $V_i(r)$, the nuclei are trapped into the pocket and fuse. The pocket is generated by the nuclear and Coulomb potentials, while the centrifugal potential serves to terminate fusion at large impact parameters. The transmission coefficients depend primarily on the energy difference, $V_i(r) - E_{c.m.}$, a sharp cutoff in angular momentum follows, and the systems behave classically. (Reviews of heavy-ion fusion containing extensive citations to the literature are given by Birkelund *et al.*,¹ Krappe,² and Vaz *et al.*³)

The character of the fusion process changes at subbarrier energies, and for heavy systems. From near-barrier and subbarrier evaporation-residue data,³⁻⁶ we find that there is more near-barrier and subbarrier fusion, especially for massive systems, than can be accounted for by penetration of the barrier $V_i(r)$, and there are pronounced variations among excitation functions, at far subbarrier energies, which are not due to barrier height or size differences. The subbarrier measurements probe³⁻⁸ those not-yet-understood early stages of the process by which cold nuclei come together and fuse.

The dominant feature of the fusion process for heavy systems is its rapid decline, as a fraction of the total reaction, with increasing mass. This steep decline is seen^{9,10} as a consequence of dynamic deformation brought on by the large Coulomb forces. Additional energy is then needed, over that given by $V_i(r)$ considerations, to drive the system over the appropriate saddle point to fusion. The complex situation in several shape degrees of freedom plus an angular momentum

dependence was reduced to a simple, classical prescription in Ref. 10. There, the additional, or extra-push, energy ΔE for a head-on collision was specified in terms of an effective entrance channel fissility $(Z^2/A)_{\text{eff}}$ by

$$\Delta E = \alpha[(Z^2/A)_{\text{eff}} - \beta]^2, \quad (Z^2/A)_{\text{eff}} > \beta, \quad (1)$$

with

$$(Z^2/A)_{\text{eff}} = 4Z_P Z_T / A_T^{1/3} A_P^{1/3} + A_P^{1/3}. \quad (2)$$

In Eq. (1), β is the critical effective fissility, the threshold in $(Z^2/A)_{\text{eff}}$ for the extra-push energy; $\alpha = cF(A_T, A_P)a^2$; and a is the slope constant governing the rate of increase in extra radial velocity. Recently,¹¹ decreasing upper limits to fission were measured for ^{208}Pb fusion with a sequence of increasingly heavier targets ranging from ^{27}Al to ^{64}Ni . These upper limits, and those examined by Sikora *et al.*,¹² were found to be systematically lower than values obtained with standard models, and support the scaling procedure of Ref. 10.

In this work we report results of measurements of cross sections for evaporation-residue formation following complete fusion for symmetric $^{90}\text{Zr} + ^{90}\text{Zr}$ and $^{90}\text{Zr} + ^{94}\text{Zr}$ systems down to far subbarrier energies. Our objective was to probe both the early, weak-contact stages of the fusion process and the later, deeper-interpenetration stages. While heavy, the $^{90}\text{Zr} + ^{90,94}\text{Zr}$ systems have fission barriers which were high enough to enable us to determine the excitation functions for complete fusion from the evaporation-residue data. The effective fissilities for these systems (Table I) are well above the threshold value $\beta = 33 \pm 1$ deduced from the compound fission data, and are considerably greater than the values 24.5 to 27.7 spanned by our earlier Ni-Ni to Ge-Ge data.

The experiments were carried out at the Brookhaven National Laboratory tandem Van de Graaff

TABLE I. Fusion and fission characteristics.

Systems	Compound nucleus	V_0 (MeV)	$(Z^2/A)_{\text{eff}}^a$	ΔE^b (MeV)	X^c	B_{fiss}^d (MeV)
$^{90}\text{Zr} + ^{94}\text{Zr}$	^{184}Hg	187.6	34.8	3.15	0.639	11.2
$^{90}\text{Zr} + ^{90}\text{Zr}$	^{180}Hg	189.0	35.6	6.45	0.645	9.9

^aEquation (2) (Ref. 13).

^bEquation (1) with $F = A_T^{1/3}A_P^{1/3}(A_T^{1/3} + A_P^{1/3})^2/(A_T + A_P)$, $ca^2 = 0.109$, $a = 12$, $\beta = 33$.

^c $X \equiv E_c^{(0)}/2E_s^{(0)} = 3e^2Z^2/10r_0c_sA$ with (Ref. 14) $r_0 = 1.16$ fm, $c_s = a_s(1 - \kappa I^2)$, $a_s = 21.14$, $\kappa = 2.4$, and $I \equiv (N-Z)/A$.

^dRef. 15.

accelerator facility, where 333- to 366-MeV ^{90}Zr beams were used to bombard thin 120- to 160- $\mu\text{g}/\text{cm}^2$ $^{90,94}\text{Zr}$ targets. Differential cross sections for the evaporation residues were measured at zero degrees in 0.5-MeV (c.m.) steps using the Massachusetts Institute of Technology-Brookhaven National Laboratory velocity selector system together with a gas ΔE , solid-state E , counter telescope.

Both source and targets were fabricated from reduced Zr powder enriched to 99.36% for ^{90}Zr and 98.58% for ^{94}Zr . The $^{90}\text{Zr} + ^{90}\text{Zr}$ data were corrected for contributions from heavier Zr isotopes with use of the $^{90}\text{Zr} + ^{94}\text{Zr}$ results, while the $^{90}\text{Zr} + ^{94}\text{Zr}$ data contained negligible contributions from the 0.12% ^{96}Zr . At 360 MeV, for example, the beam intensity was 0.75 e-nA, the terminal voltage was 16.5 MV, and the double-stripping charge-state combination was $14^+/23^+$. The velocity selector system consisted of an electrostatic beam separator followed by an $E \times B$ velocity filter, plus fore and aft magnetic quadrupole doublets. Absolute cross sections were obtained by normalizing the evaporation-residue yields to Rutherford scattering yields detected in two target-chamber solid-state detectors. The zero-degree differential cross sections were converted to cross sections for evaporation-residue formation with results of an angular distribution measurement, supplemented by detailed Monte Carlo calculations of recoil properties.

The resulting cross sections for the $^{90}\text{Zr} + ^{94}\text{Zr}$ and $^{90}\text{Zr} + ^{90}\text{Zr}$ systems are displayed in Fig. 1. At the highest energies in the vicinity of the nominal fusion barrier, the cross sections for the $^{90}\text{Zr} + ^{94}\text{Zr}$ system are on the order of a millibarn. These cross sections drop off gradually, at first, reaching the 100- μb level 13 MeV (c.m.) below the barrier, and then with increasing steepness, reaching the 1- μb level 18 MeV below V_0 .

The behavior of the $^{90}\text{Zr} + ^{90}\text{Zr}$ cross sections is similar except the steepness of the dropoff is greater, reaching the 600-nb level 15 MeV below the nominal fusion barrier. The nominal fusion barriers for the systems are listed in column 3 of Table I. These quantities represent the s-wave interaction barrier maxima for spherical nuclei as calculated with the generalized liquid-drop potential of Krappé *et al.*¹⁶

The fissilities are listed in Table I, column 6, and the fission-barrier heights are given in column 7. The high values for B_{fiss} , plus the low excitation energies in the $^{184}\text{Hg}^*$ and $^{180}\text{Hg}^*$ com-

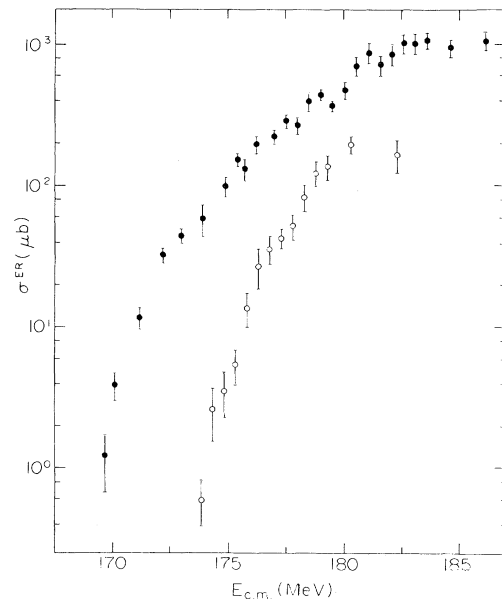


FIG. 1. Plot of cross sections for evaporation-residue formation following fusion of ^{90}Zr with ^{90}Zr (open circles) and ^{94}Zr (filled circles) vs average center-of-mass energy. Error bars denote statistical errors. Uncertainties in absolute cross sections are 20% for ^{90}Zr and 12% to 15% for ^{94}Zr .

pound nuclei, ensure that the fission branching ratios and multiple-chance fission contributions are small. Measurements of both σ^{ER} and σ^{fiss} have been performed¹⁷ for the $^{40}\text{Ar} + ^{144}\text{Sm} \rightarrow ^{184}\text{Hg}^*$ system. The fission cross sections were found to be about one-third of σ^{CF} below the barrier, and about one-half of σ^{CF} in the vicinity of the barrier. For the $^{90}\text{Zr} + ^{94}\text{Zr}$ system two methods of adding the fission contributions were used. In one, the evaporation-residue cross sections were multiplied by $(\sigma^{\text{ER}} + \sigma^{\text{fiss}})/\sigma^{\text{ER}}$ determined from the $^{40}\text{Ar} + ^{144}\text{Sm}$ data; in the other, multiple-chance-fission/particle-emission calculations were performed. This latter approach was used for the $^{90}\text{Zr} + ^{90}\text{Zr}$ system, as well.

In Fig. 2 the excitation functions for complete fusion for the $^{90}\text{Zr} + ^{90,94}\text{Zr}$ systems are compared with the excitation functions for complete fusion for the $^{58}\text{Ni} + ^{58}\text{Ni}$ (Ref. 4) and $^{74}\text{Ge} + ^{74}\text{Ge}$ (Ref. 18) systems. We see that the excitation function for the $^{90}\text{Zr} + ^{94}\text{Zr}$ system is shifted downward from

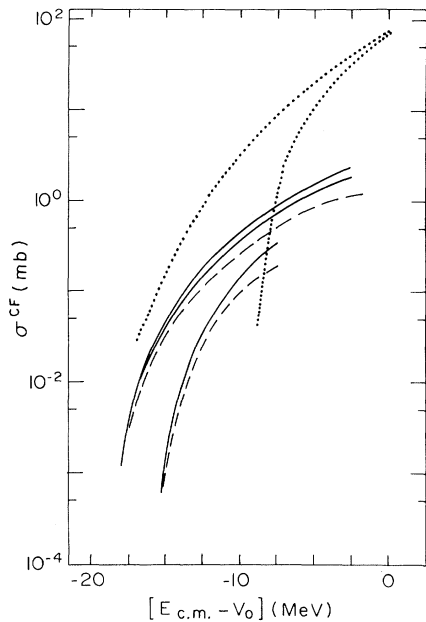


FIG. 2. Plot of excitation functions for complete fusion vs the difference between the average center-of-mass energies and the fusion-barrier height calculated with the Krappé-Nix-Sierk potential (Ref. 16). Dotted lines denote the excitation functions for $^{58}\text{Ni} + ^{58}\text{Ni}$ (Ref. 4) (lower curve) and $^{74}\text{Ge} + ^{74}\text{Ge}$ (Ref. 18) (upper curve). Dashed lines represent the evaporation residue data for $^{90}\text{Zr} + ^{90}\text{Zr}$ (lower curve) and $^{90}\text{Zr} + ^{94}\text{Zr}$ (upper curve); solid lines denote the corresponding complete-fusion excitation function [for $^{90}\text{Zr} + ^{94}\text{Zr}$, upper line denotes scaled results, and lower line denotes calculated (Ref. 19) results].

those for the $^{58}\text{Ni} + ^{58}\text{Ni}$ and $^{74}\text{Ge} + ^{74}\text{Ge}$ systems by a factor of 20 in the vicinity of V_0 . In the standard approach, the partial fusion cross sections, σ_i , are given by $\sigma_i = \pi \lambda^2 (2l+1) T_l$, where λ is the reduced de Broglie wavelength of the incident ion and T_l is the transmission coefficient. The expected value for σ^{CF} at the barrier V_0 is ~ 10 mb. This value occurs, by extrapolation of the $^{90}\text{Zr} + ^{94}\text{Zr}$ excitation function displayed in Fig. 2, at an energy $\Delta E = 10.5 \pm 3.0$ MeV higher than the nominal V_0 . This is in sharp contrast to what happens in the Ni to Ge region, where fitted fusion barriers were 4 to 6 MeV lower than the nominal V_0 .

We also observe in Fig. 2 that the gentle decline in the $^{90}\text{Zr} + ^{90,94}\text{Zr}$ excitation functions extends to energies more than 10 MeV below the barrier. The difference in slope between the excitation functions for $^{90}\text{Zr} + ^{94}\text{Zr}$ and $^{58}\text{Ni} + ^{58}\text{Ni}$ is pronounced. Recall, furthermore, that the steeper decline in the $^{58}\text{Ni} + ^{58}\text{Ni}$ excitation function is, in fact, more gradual than that given by standard barrier-penetration models. These Zr+Zr systems seem to have narrow effective barriers and/or small effective masses along the dynamic path leading to fusion. If the subbarrier process is nearly adiabatic, then the relative ease with which fusion occurs may result¹⁰ from superfluidity of the cold, heavy nuclei, manifesting itself when the nuclei come into weak contact.

By interpreting the positive ΔE as an extra-push energy, we obtain a critical effective fissility $\beta = 31.5 \pm 0.5$ (using $a = 12$). This may be compared to $\beta = 33 \pm 1$ deduced¹⁰ from the fission data of Ref. 11 involving a different mass asymmetry and angular momentum regime. In addition to expecting⁴ neutron transfer/exchange processes during weak contact, one anticipates an increased probability for coalescence/reseparation during deeper interpenetration. The decreased fusion at and above the nominal barrier would then reflect the increased competition for the low partial waves by reaction processes such as massive transfer and deep-inelastic collisions.

To summarize, we have measured cross sections for evaporation-residue formation following complete fusion of ^{90}Zr with $^{90,94}\text{Zr}$ down to subbarrier energies. While the effective fusion barrier for the $^{90}\text{Zr} + ^{94}\text{Zr}$ system is 10.5 ± 3.0 MeV higher than the nominal barrier, the complete-fusion excitation function decreases slowly over a broad energy range below the barrier. From the difference between effective and nominal fusion barriers we extracted a critical effective

fissility $\beta = 31.5 \pm 0.5$. Although fusion at near-barrier energies seems to be influenced by what happens during deep interpenetration, at lower energies the weak-contact dynamics enable these cold, heavy nuclei to fuse with relative ease.

This work was supported by the U. S. Department of Energy under Contract No. DE-AC02-76ERO3069.

¹J. R. Birkelund *et al.*, Phys. Rep. **56**, 107 (1979).

²H. J. Krappe, in *Deep Inelastic and Fusion Reactions with Heavy Ions*, edited by W. von Oertzen, Lecture Notes in Physics Vol. 117 (Springer-Verlag, New York, 1980), p. 312.

³L. C. Vaz *et al.*, Phys. Rep. **69**, 373 (1981).

⁴M. Beckerman *et al.*, Phys. Rev. Lett. **45**, 1472 (1980), and Phys. Rev. C **23**, 1581 (1981), and **25**, 837 (1982).

⁵D. Evers *et al.*, in Proceedings of the Nineteenth International Winter Meeting on Nuclear Physics, Bormio, 1981 (unpublished).

⁶U. Jahnke *et al.*, Phys. Rev. Lett. **48**, 17 (1982).

⁷H. Esbensen, Nucl. Phys. **A352**, 147 (1981).

⁸S. Landowne and J. R. Nix, Nucl. Phys. **A368**, 352 (1981).

⁹J. R. Nix and A. J. Sierk, Phys. Rev. C **15**, 2072 (1977).

¹⁰W. J. Swiatecki, Nucl. Phys. **A376**, 275 (1982), and Phys. Scr. **24**, 1248 (1981).

¹¹H. Sann *et al.*, Phys. Rev. Lett. **47**, 1248 (1981).

¹²B. Sikora *et al.*, Phys. Rev. C **25**, 686 (1982).

¹³R. Bass, Nucl. Phys. **A231**, 45 (1974).

¹⁴P. Möller and J. R. Nix, Nucl. Phys. **A361**, 117 (1981).

¹⁵A. J. Sierk, private communication.

¹⁶H. J. Krappe *et al.*, Phys. Rev. Lett. **42**, 215 (1979), and Phys. Rev. C **20**, 992 (1979).

¹⁷R. G. Stokstad *et al.*, Z. Phys. A **295**, 269 (1980).

¹⁸M. Beckerman *et al.*, to be published.

¹⁹Calculations performed with the code MB-II [M. Beckerman and M. Blann, Phys. Rev. C **17**, 1615 (1978), and University of Rochester Report No. UR-NSRL-135, 1977 (unpublished)] with $a_f/a_v = 1.08$, and rotating-liquid-drop fission barriers adjusted to the $I = 0$ value in Table I.

Rejection of Evidence for Nonzero Neutrino Rest Mass from Double Beta Decay

T. Kirsten, H. Richter, and E. Jessberger

Max-Planck-Institut für Kernphysik, D-6900 Heidelberg, Germany

(Received 1 October 1982)

Previous evidence from double beta decay (DBD) of ^{128}Te and ^{130}Te required neutrinoless DBD involving a neutrino rest mass of $\hat{m}_\nu \sim 34$ eV (~ 10 eV in the most recent theoretical treatment) or else a strong violation of lepton-number conservation ($\eta \neq 0$) due to a ($V + A$) admixture. The DBD rate ratio of ^{128}Te and ^{130}Te has been redetermined. The present result is consistent with $\hat{m}_\nu = \eta = 0$. The experimental limits still allow Majorana decay at levels of $\hat{m}_\nu \leq 5.6$ eV or $\eta \leq 2.4 \times 10^{-5}$ (95% confidence). The DBD half-life for ^{128}Te is $T_{1/2}(^{128}\text{Te}) > 8 \times 10^{24}$ yr (2σ).

PACS numbers: 23.40.Bw, 14.60.Gh, 27.60.+j

Double beta decay (DBD) may occur with neutrino emission (2ν , Dirac decay) or without neutrinos (0ν , Majorana decay). Neutrinoless DBD is made possible either by a right-handed leptonic current admixture¹ (violation of lepton-number conservation, amplitude η) or by an implicit helicity breaking due to a nonzero mass of the electron neutrino ($\hat{m}_\nu \neq 0$).²⁻⁴ The presence or absence of measurable decay rates $\lambda_{0\nu}$ puts stringent limits on η and \hat{m}_ν . Even very small values of η, \hat{m}_ν lead to effectively enhanced decay rates since Majorana decay is promoted by a phase-space factor $\sim 10^6$ relative to Dirac decay. DBD is thus considered to be "the most sensitive test for lepton-quark symmetry."⁵

DBD has been experimentally observed so far by the geochemical method.⁶⁻¹¹ This method yields effective decay rates $\lambda_\Sigma = \lambda_{0\nu} + \lambda_{2\nu}$ and one cannot distinguish between Majorana and Dirac decay. Limits on η have nevertheless been inferred from $\lambda_{0\nu} < \lambda_\Sigma$. These limits suffered, however, from the uncertainties of the nuclear matrix elements and hence the theoretical decay-rate predictions. Pontecorvo¹² pointed out that the situation is much improved if decay-rate ratios of similar nuclei such as ^{128}Te - ^{130}Te (or ^{80}Se - ^{82}Se) are considered because the ratio of their respective relevant nuclear matrix elements should be near unity. In addition, the ratio $\rho_{0\nu} = {}^{128}\lambda_{0\nu} / {}^{130}\lambda_{0\nu}$ becomes much larger than